HANDBOOK OF
SCALING METHODS IN AQUATIC ECOLOGY
MEASUREMENT, ANALYSIS, SIMULATION

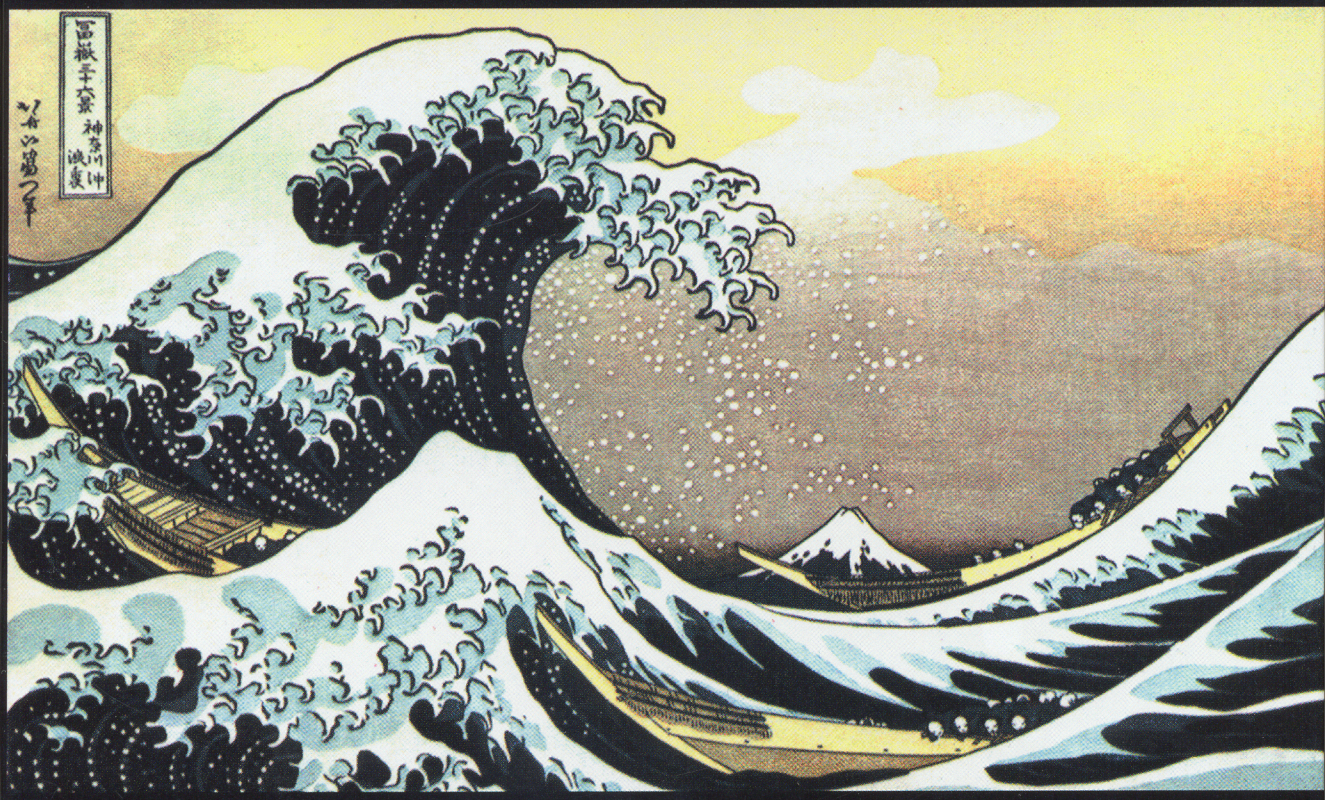

EDITED BY
LAURENT SEURONT
PETER G. STRUTTON

CRC PRESS

Cover: *Mount Fuji from the Offing*, also known as *The Great Wave off Kanagawa*, from the series of block prints *36 Views of Mount Fuji* (1823–1829) by Katsushika Hokusai (1760–1849).

Senior Editor: John Sulzycki
Production Editor: Christine Andreasen
Project Coordinator: Erika Dery
Marketing Manager: Nadja English

Library of Congress Cataloging-in-Publication Data

Handbook of scaling methods in aquatic ecology : measurement, analysis, simulation / edited by Laurent Seuront and Peter G. Strutton.
p. cm.
Includes bibliographical references and index.
ISBN 0-8493-1344-9
1. Aquatic ecology—Research—Methodology. 2. Aquatic ecology—Measurement. 3. Aquatic ecology—Simulation methods. I. Seuront, Laurent. II. Strutton, Peter G.

QH541.5.W3H36 2003
577.6'072—dc21 2003051467

Visit the CRC Press Web site at www.crcpress.com

International Standard Book Number 0-8493-1344-9
Library of Congress Card Number 2003051467
Printed in the United States of America 1 2 3 4 5 6 7 8 9 0
Printed on acid-free paper

11

Experimental Validation of an Individual-Based Model for Zooplankton Swarming

Neil S. Banas, Dong-Ping Wang, and Jeannette Yen

CONTENTS

11.1 Introduction

The ecology of marine planktonic assemblages depends, in essential, intricate ways, on the behavior of individual zooplankters. Swarming behavior is among the most crucial, and also least charted, of the territories that span population and organismal biology in this way. On large scales in the ocean, and possibly in some small-scale environments like frontal zones, aggregation into patches is probably a physics-driven, passive process. At the same time, active swarming behavior — that is, a type of motion that resists dispersion without orienting or distributing animals in an organized way — is well known,

0-8493-1344-9/04/$0.00+$1.50

and controls small-scale zooplankton distribution in the ocean to an unknown extent. Passive and active aggregations are essential for setting encounter rates between predators and prey, between grazers and patchily distributed food sources (Lasker, 1975; Davis et al., 1991) and between conspecifics in search of mates (Brandl and Fernando, 1971; Hebert et al., 1980; Gendron, 1992).

Swarming differs from schooling (which is known but rare among the zooplankton; Hamner et al., 1983) in that it is stochastic, unarrayed, and largely uncoordinated between individuals. At the same time swarming differs from truly random motion — that is, Brownian motion or diffusion — in that a swarm does not spread out over time and disperse as does a cloud of molecules or drifting particles. Behaviors that maintain swarms against diffusion may be either social and density dependent or nonsocial and density independent; we consider each category briefly in turn.

A variety of models for social swarm maintenance have been proposed, centered on mechanisms in which, for example, animals seek a target density (Grünbaum, 1994) or correlate their motion with their neighbors' motion (Yamazaki, 1993). The possibilities for such mechanisms in a given species are strongly constrained by sensory ability. Perhaps the most fundamental constraint is that the majority of zooplankton lack image-forming eyes (Eloffson, 1966) and, accordingly, do not appear to orient to their conspecifics visually. Long-distance interactions along scent trails have been observed in copepod swarms (Katona, 1973; Weissburg et al., 1998), and similar interactions are possible along trails in the shear or pressure fields (Fields and Yen, 1997), as has been observed in schools of Antarctic krill (Hamner et al., 1983). Nevertheless, most intraspecies communication in zooplankton appears to be local and intermittent, as opposed, say, to the long-range and constant visual coordination that gives fish schools their character. Leising and Yen (1997), for example, found five copepod species to be insensitive to the proximity of their conspecifics except at nearest-neighbor distances of a few body lengths. Swarms of this density are rarely found in nature (Alldredge et al., 1984). It is important to note that even intermittent social interactions may play a large role in swarm dynamics. Leising and Yen argue that the number density of the laboratory swarms they observe is controlled by avoidance reactions to chance close-range encounters in the swarm center.

A number of nonsocial aggregative behaviors have also been observed *in situ*. Phototaxis maintains swarms of the cyclopoid copepod *Dioithona oculata* in shafts of light between mangrove roots (Ambler et al., 1991), and similar responses to light gradients are known in several other species (Hamner and Carlton, 1979; Hebert, 1980; Ueda et al., 1983). Attraction to food odors, and increased turning in food patches, which aids foraging and increases forager density, have also been observed in a number of species (Williamson, 1981; Poulet and Ouellet, 1982; Tiselius, 1992; Bundy et al., 1993). Some zooplankton in fact may respond directly to water temperature and salinity (Wishner et al., 1988; Gallager et al., 1996).

This enormous range of social and individual behaviors does not consolidate readily into a simple, general account of zooplankton swarming. Still, a unifying thread runs through them: whatever the driving behavioral mechanism, the tendency that counters dispersion in a swarm is not just a collective, statistical property, but rather must be observable in each swarmer's individual motion as a hidden regularity. This is an experimentally powerful notion, for it suggests that we may be able to apprehend the dynamics of a large, observationally unwieldly aggregation by studying the behavior of a few typical individuals. Indeed, in a dynamic, rather than statistical (one could also say ethological, rather than ecological) approach to animal swarming, the larger aggregation may often be close to irrelevant. Writes Okubo (1986):

> There is an interesting observation by Bassler that a swarm could be reduced to a single individual of mosquito, *Culex pipiens* which yet continued to show the characteristic behavior of swarming dance [Clements, 1963]. Also Goldsmith et al. [1980]... noted that a single and a few midges did show movements characteristic of swarming by a large number of animals.

Provocatively, many zooplankton may behave like mosquitoes and midges in this respect, and form swarms in which interaction between individuals plays at most a secondary role. Yen and Bundock (1997), for example, found no social interaction within phototactic laboratory swarms of the harpactacoid copepod *Coullana canadensis*.

When interaction does occur, as noted above, it is generally chemical or rheotactic, rather than visual, and thus occurs slowly, along spatially torturous paths. These paths are very difficult to observe or map, and in a large aggregation, especially outside the laboratory, would not easily be differentiated from a diffuse, continuous sensory cue. Indeed, if such interactions are fundamental to the dynamics of a swarm (as opposed to simply being facilitated by the swarm, as mating encounters might be), then their importance is not particular but cumulative, statistical, parameterizable. While the details of social communication are crucially relevant to swarming biology on one level, for analyzing balances between dispersion and counterdispersion — for understanding the kinematics of an individual swarmer — it seems more apt to average over many encounters, and to model social effects as a net dispersive or concentrative tendency in each individual.

In this modeling approach, then, whether a swarm is socially or nonsocially driven, we regard it as an interaction not between animals, but between each animal and its local stimulus field. This approach has the advantage of generality. While one can parameterize a social, density-dependent response — a series of avoidance reactions, for example, or motion through a network of pheromonal trails — as an individual response to a steady cue, it is hard to imagine modeling, say, phototaxis by reversing the analogy.

Attempts to produce a general quantitative description of zooplankton swarming have been frustrated by a lack of marine observations. Okubo and Anderson (1984) present a simple and general individual-based model of steady-state swarming (see also Okubo, 1980, 1986), but write that for purposes of model verification, "no such data really exist in the marine field." They proceed, with reservations, by examining data from "aeroplankton," midges swarming in a forest clearing. Since the time of their publication, optical and acoustic technologies for observing and recording *in situ* zooplankton distribution and behavior have become available (Alldredge et al., 1984; Schultze et al., 1992; Smith et al., 1992; Davis et al., 1992). These and laboratory methods have occasionally been applied to the problem of aggregation dynamics. McGehee and Jaffe (1996), for example, examine the relationship between path curvature and swimming speed in a zooplankton patch observed through acoustic imaging; Buskey et al. (1995) used three-dimensional imaging in the laboratory to analyze the phototactic formation of a swarm in *Dioithona oculata.*

Still, no dynamic account has been given of the swarming motion of individual animals followed for sustained periods. In the present study we use optical methods developed by Strickler (1998) to evaluate Okubo and Anderson's model — the "aggregating random walk" (Yamazaki, 1993) — in the case of two species of zooplankton, the calanoid copepod *Temora longicornis* and the cladoceran *Daphnia magna*, swarming phototactically in the laboratory.

11.2 Theory

In this section we derive quantitative predictions of the aggregating random-walk model, which we can directly compare with data, beginning from kinematic first principles, following Okubo and Anderson (1984).

11.2.1 Differentiating between Swarming and Diffusion

Assume for simplicity that the swarming motion is one dimensional, in the x direction — we generalize to two and three dimensions later — and assume that the swarm has reached a steady state and is isotropic. If all the swarmers are responding to the attractive stimulus in the same way, then their paths will be centered on the same point: call this the origin. Then the spatial variance $\overline{x^2}$ of an individual's path also measures the size of the swarm.

A standard result in the theory of diffusion (Okubo, 1980) is that under these assumptions, for large t, $\overline{x^2}$ increases as

$$\overline{x^2} \to 2Dt \tag{11.1}$$

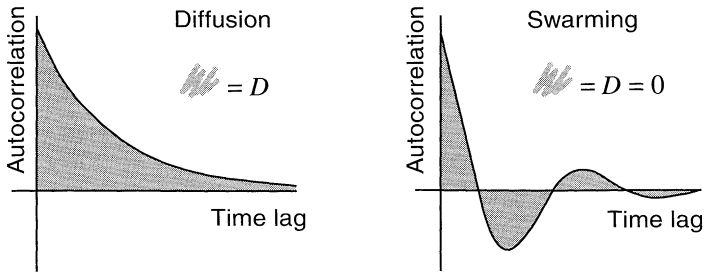

FIGURE 11.1 Schematic representation of the distinction in velocity autocorrelations between swarming and diffusion. The shaded area in each case is equal to the diffusion coefficient D.

where D is the diffusivity. D can be written as

$$D \equiv \overline{u^2} \int_0^\infty R(\tau) d\tau \tag{11.2}$$

where $u \equiv dx/dt$. R is the Lagrangian velocity autocorrelation coefficient, a function of time lag τ:

$$R(\tau) \equiv \frac{1}{\overline{u^2}} \overline{u(t)u(t+\tau)} \tag{11.3}$$

Eventually any individual's velocity decorrelates from its earlier values, since no animal, swarming, diffusing, or otherwise, moves in the same pattern forever, and so $R(\tau) \to 0$ for large τ. The shape of $R(\tau)$ as it tends to this asymptotic limit, however, is variable. In the case of simple diffusion, $R(\tau)$ decays exponentially. Its integral is a positive number, so that D, by Equation 11.2, is a positive number, and $\overline{x^2}$, by Equation 11.1, increases linearly. In the case of swarming, in which trajectories do not spread over time, however, $\overline{x^2}$ remains constant; D must then be zero; and $R(\tau)$ oscillates about the axis in such a way that its area converges likewise to zero (Figure 11.1).

Thus the shape of $R(\tau)$ — specifically, the presence or absence of an axis crossing — is the key to distinguishing kinematically between swarming animals and diffusing ones. $R(\tau)$ can be calculated directly from position and velocity data by Equation 11.3.

11.2.2 Diffusion in an Aggregative Force Field

We can recast the problem in dynamic Newtonian terms, again following Okubo and Anderson, as a balance between diffusion and a deterministic concentrative force. In this model the concentrative force, an inward acceleration that grows with distance from an attractor at the swarm center, keeps the swarmers from dispersing, while diffusive motion keeps the swarmers from collapsing onto the central attractor.

The resulting equation of motion can be written:

$$du/dt = A - ku - \omega^2 x \tag{11.4}$$

The first two terms on the right-hand side constitute a standard "random-flight" model of diffusion: k is a frictional coefficient in a Stokes model of drag, and $A(t)$ is a random acceleration, some sort of white noise, with a delta-function autocorrelation and finite power $B \equiv \overline{Au}$. Note that we can interpret this random excitation and frictional damping either as true external, turbulent forces acting upon a passive particle, or simply as accelerations that express behavior patterns.

The third term on the right-hand side, the concentrative force, can be interpreted either as a harmonic (linear) restoring force, such as the force that gravity exerts on a pendulum, or as a local approximation to a more complicated, anharmonic restoring force. Okubo and Anderson suggest anharmonicity as a mechanism for maintaining a uniform, rather than Gaussian, density distribution through the swarm center. Our experiment neither confirms nor refutes this idea, and so in the interest of empiricism we have retained only the harmonic concentrative term. We view our dynamic model (Equation 11.4) as a

first-order approximation to a behavior that may well involve a number of unmodeled, higher-order effects, such as advection of momentum, in both the diffusive and concentrative motions. Higher-order models may be necessary to parameterize the effects of foraging, mate-finding, escapes, and other behaviors simultaneous with swarming.

As shown by Okubo (1986), Equation 11.4 does indeed yield a velocity autocorrelation of the form required by kinematic considerations, as discussed above and illustrated in Figure 11.1:

$$R(\tau) = e^{-k\tau/2}\left(\cos\omega_1 t - \frac{k}{2\omega_1}\sin\omega_1 t\right) \tag{11.5}$$

where

$$\omega_1^2 = \omega^2 - k^2/4 \tag{11.6}$$

The integral of $R(\tau)$ is identically zero. Note that as the attractive forcing weakens — that is, as $\omega \to 0$ — Equations 11.4 and 11.5 both approach the results for simple diffusion:

$$du/dt = A - ku \tag{11.7}$$

$$R(\tau) = e^{-k\tau} \tag{11.8}$$

In practice, we necessarily calculate the autocorrelation $R(\tau)$ on discrete time series, either from experiment or from numerical simulation, and such a discrete autocorrelation is not fully equivalent to Equation 11.5, derived from continuous dynamics. Yamazaki and Okubo (1995) show that the discrete autocorrelation does not integrate to zero, i.e., that discretization introduces an apparent (but artificial) net diffusion rate. This mathematical inconsistency is potentially a limit on the precision with which we can determine k and ω from observations.

11.2.3 Further Model Predictions

In this model, a swarm is characterized primarily by position variance $\overline{x^2}$ (a measure of the size of the swarm), velocity variance $\overline{u^2}$ (a measure of the kinetic energy of its members) and by k, ω, and B (measures of the strength of the damping, attractive, and excitational forces). We can derive from Equation 11.4 some useful and experimentally verifiable relationships between these parameters.

Multiplying Equation 11.4 by u and taking the time average, we obtain

$$\overline{u\frac{du}{dt}} = -\overline{ku^2} - \omega^2\overline{xu} + \overline{Au} \tag{11.9}$$

$\overline{Au}$ is the power of the random forcing, or B. Since we assume the swarm is in a steady state, both $\overline{u(du/dt)}$ and $\overline{x(dx/dt)}$ are zero. Thus, Equation 11.9 becomes

$$\overline{u^2} = \frac{B}{k} \tag{11.10}$$

Note that this relationship is independent of ω and therefore true of purely diffusive motion as well. Thus the attractive force has no bearing on the kinetic energy of a swarm. Nor does it influence the speed distribution of the swarmers: an individual subject to Equation 11.3 follows the Maxwellian speed distribution for free particles (like gas molecules):

$$p(u) = \frac{1}{\sqrt{2\pi\overline{u^2}}}\exp\left(-\frac{u^2}{\overline{u^2}}\right) \tag{11.11}$$

where $p(u)$ is the fraction of a statistical ensemble found between velocities u and $u + du$ (Okubo and Anderson, 1984).

The strength of the attractive force does, however, have a very direct bearing on the steady-state swarm size $\overline{x^2}$. For large t, $\overline{x^2}$ approaches the value

$$\overline{x^2} = \frac{\overline{u^2}}{\omega^2} \tag{11.12}$$

(Uhlenbeck and Ornstein, 1930). Thus swarm size is inversely proportional to the strength of the attractive forcing. When ω is large — that is, when the attractive tendency increases rapidly with distance from the swarm center — the swarm is concentrated tightly. As ω approaches zero — the case of pure diffusion — the swarm's limiting size increases toward infinity.

11.2.4 Swarming in Two and Three Dimensions

These results can easily be generalized to more than one dimension. Assume, for example, that the same forces that act in the x direction act in the y. Because our model involves no coupling of motion along different axes, the results so far derived still hold, and $\overline{y^2}$ and $\overline{v^2}$ (where $v \equiv dy/dt$) are related to k and ω by expressions analogous to Equation 11.10 and 11.12. We can then write expressions for the two-dimensional parameters of interest:

$$\overline{V^2} \equiv \overline{u^2} + \overline{v^2} = \frac{2B}{k} \tag{11.13}$$

$$\overline{r^2} \equiv \overline{x^2} + \overline{y^2} = \frac{\overline{V^2}}{\omega^2} \tag{11.14}$$

The generalization to three dimensions is analogous.

Velocity distributions for two- and three-dimensional swarms are simply the two- and three-dimensional Maxwellian distributions. In two dimensions,

$$p(V) = \frac{2}{\overline{V^2}} V \exp\left(-\frac{V^2}{\overline{V^2}}\right) \tag{11.15}$$

Note that animals swarming in a three-dimensional ocean are not necessarily engaged in three-dimensional swarming. The number of dimensions in which the swarming model applies depends on the symmetries of the attractor. If the attractor is planar (for example, a front or thin layer containing high food concentrations: Yoder et al., 1994; Hanson and Donaghay, 1998), then the swarming forces do indeed act in only one dimension, the vertical, and motion in the two horizontal dimensions, in which the attractor is isotropic, is likely to be diffusive. If the attractor is one dimensional (for example, the light shaft in our experiment, or a light shaft through mangrove roots: Ambler et al., 1991), then we might expect swarming motion in two dimensions and diffusive motion in the third. Only if the attractor is a point or spherically symmetrical (for example, a diffusing chemical signal in an isotropic environment) does the swarming model apply to three dimensions.

11.2.5 The Acceleration Field

Finally, returning to the one-dimensional case, we can derive predictions about the mean and variance of the spatially varying acceleration field.

Taking the mean of Equation 11.4, holding x constant, we obtain

$$\overline{a(x)} = -\omega^2 x \tag{11.16}$$

where $a \equiv du/dt$. Thus, the mean acceleration field consists of the center-directed concentrative force alone.

Fluctuations about this mean consist of the random-flight accelerations $A(t) - ku$. Okubo (1986) derives an expression for the expected variance of these fluctuations, $\overline{a^2}$. The quantity we actually calculate from data, however, is not acceleration but a finite-difference approximation to acceleration:

$$\frac{\Delta u}{\Delta t} = \frac{u(t_0 + \Delta t) - u(t_0)}{\Delta t} \tag{11.17}$$

where Δt is the sampling period, and the theoretical variance of $\Delta u/\Delta t$ is not the same as that of the acceleration itself. (Note that the distinction does not affect the predicted mean acceleration field, or the predictions concerning the velocity field given above.) Without loss of generality, set $t_0 = 0$. Then the finite-difference acceleration variance can be written

$$\begin{aligned}\overline{\frac{\Delta u^2}{\Delta t^2}} &= \frac{1}{\Delta t^2}\overline{\left[u(t_0 + \Delta t) - u(t_0)\right]\left[u(t_0 + \Delta t) - u(t_0)\right]} \\ &= \frac{1}{\Delta t^2}\left(2\overline{u^2} + 2\overline{u(t_0)u(t_0 + \Delta t)}\right)\end{aligned} \tag{11.18}$$

since the velocity variance is assumed constant in time. The second term can be evaluated using the definition of the autocorrelation (Equation 11.3) and the diffusive result (Equation 11.8), so that

$$\overline{\frac{\Delta u^2}{\Delta t^2}} = \frac{2\overline{u^2}}{\Delta t^2}\left(1 - e^{-k\Delta t}\right) \tag{11.19}$$

predicts the variance about the mean acceleration $\overline{a(x)}$ for a time series sampled with a time step Δt.

Just as the acceleration field has a finite variance about the mean, so does the autocorrelation curve $R(\tau)$. Only the mean autocorrelation was derived above. Because of the complexity of the problem, however, in the data analysis below we estimate the theoretical variance of the autocorrelation numerically, through direct integration of the equation of motion (Equation 11.4), rather than deriving an expression for it analytically.

11.3 Experiment

Data were collected for homogeneous groups of two species, the freshwater cladoceran *Daphnia magna* (Hussussian et al., 1993) and the calanoid copepod *Temora longicornus*. In each experiment the animals were placed in a small (10 × 10 × 15 cm) Plexiglas tank, a light down the center axis of the tank turned on, and the trajectories of the animals swarming to the light recorded on videotape and then digitized.

The geometry of the tank-and-light system is shown in Figure 11.2. Description of the optical methods employed can be found in Strickler and Hwang (1998) and Strickler (1998); digitization methods are

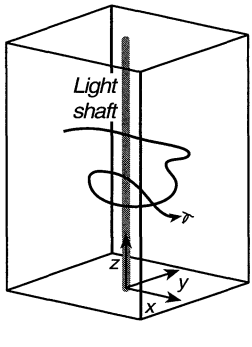

FIGURE 11.2 Geometry of the tank and light system.

described in Doall et al. (1998). The light source in the *Daphnia* experiment was a 3-mW argon laser (wavelength 488 and 514.5 nm), which produced a collimated beam 4 mm wide throughout the water column. The *Temora* experiment used a 2-mm-diameter fiber-optic light guide, projecting light from a halogen lamp at the top of the tank. This produced a narrow cone-shaped beam with more attenuation through the water column, although the beam reached clearly to the bottom of the tank.

All three axes of motion were captured for the *Temora* experiment, using a pair of orthogonal projections. One camera recorded motion in the x–z plane, and a second, motion in the y–z plane, so that by matching z motions one could recover full three-dimensional trajectories. The *Daphnia* experiment was recorded with an earlier generation of the optical system and thus contains only a single x–z projection. Because of the radial symmetry of the light source, and the fact that our model predicts no coupling of motion between orthogonal axes, the lack of a third dimension in the *Daphnia* data does not hinder the statistical analysis.

Phototaxis in marine and freshwater macrozooplankton is well known, primarily in the context of light-gradient-driven diel migration (Russell, 1934; Stearns, 1975; Bollens et al., 1994). The behavioral significance of the strong positive phototaxis that zooplankters often show in the laboratory, however, is poorly understood. Some animals placed in the tank showed no attraction to the light, and the response of other animals was intermittent. Some of the *Temora* simply remained at the bottom of the tank, while others collected at the surface, where the fiber-optic illumination was intensified. Flux between these subpopulations and the swarm in the mid-water column was continual. Trajectories for analysis were taken from the animals that remained in the swarm for longer than one sample period.

These swarms tended to be small, generally consisting of fewer than ten animals, so that mean nearest-neighbor distances were many body lengths. This low density is consistent with our treatment of swarming behavior not as a density-dependent, social interaction, but rather as an individual response to a sensory cue. The simultaneity or nonsimultaneity of the swarmers' motions does not enter into the analysis, because each animal is in effect swarming alone.

11.4 Analysis

11.4.1 Constructing a Statistical Ensemble

Trajectories were sampled at 1-s intervals. This time step was chosen both to resolve the fundamental timescales of motion (the damping time $1/k$ and the attractive force period $2\pi/\omega$, which were estimated by an initial calculation of the velocity autocorrelation) and simultaneously to filter out higher-frequency behaviors such as avoidance reactions and trail following (Weissburg et al., 1998). Long-time step sampling is an unrefined method for low-pass-filtering a trajectory record; but a test performed on *Temora* data sampled at 0.2 s suggested that the choice of this method over tapered low-pass filtering of a higher-resolution data set had a negligible effect on the analysis. Longer-time step sampling makes the digitization of trajectories (which was done by hand here rather than by computer program to ensure accuracy) far less labor intensive.

Recorded trajectories were divided into uniform 20-s segments for the analysis. This length of time was chosen to balance two considerations. The segments had to be long enough to resolve the inherent dynamic timescales mentioned above, and at the same time as short as possible — i.e., as close to the autocorrelation timescale as possible — to ensure uniformity of behavior within each record. They thus become independent samples in the statistical sense. Within each 20-s segment, velocities and accelerations were calculated using the finite-difference equations

$$u(t) \sim \frac{x(t) - x(t - \Delta t)}{\Delta t} \tag{11.20}$$

$$a(t) = \frac{u(t + \Delta t) - u(t)}{\Delta t} = \frac{x(t + \Delta t) - 2x(t) + x(t - \Delta t)}{\Delta t^2} \tag{11.21}$$

Even among the animals that remained suspended in the water column, not all were engaged in swarming behavior. A few simply drifted through the swarm without, in a kinematic sense, being part of it, like waiters carrying trays across a lively ballroom. The shape of the velocity autocorrelation, as illustrated in Figure 11.1, quantitatively distinguishes swarmers from drifters, i.e., slow diffusers. As our goal is not to test a hypothesis about the phototactic behavior of *Daphnia* and *Temora*, but rather to describe the swarming that a light gradient *can* evoke in these animals, we winnowed the trajectory set to remove those animals who were not participating. (Because this winnowing eliminated only a small number of candidate trajectories, as described below, it is fair to assume that the swarming dynamics thus described account for the bulk of the animals' response to this stimulus.) We eliminated from both the *Daphnia* and *Temora* data sets trajectory samples whose velocity autocorrelation did not cross the time axis, as well as samples whose mean position lay more than two standard deviations from the z axis, the swarm center. These criteria eliminated 4 of 24 *Temora* trajectories and 2 of 60 *Daphnia* trajectories. Some diffusers were also eliminated by eye before digitization of trajectories began. Lateral projections of all remaining *Daphnia* and *Temora* trajectories are shown superimposed in Figure 11.3A and Figure 11.4A, B.

The final step in creating a uniform statistical ensemble of trajectories is to verify that the process captured is kinematically stationary. Figure 11.3B and Figure 11.4C show the means and standard deviations of position and velocity for both data sets. Note that there are no strong outliers, and that the variances of the ensembles are on the same order as the variances of individual trajectories within them.

11.4.2 A Procedure for Testing Model Consistency

We proceed as follows for both the *Daphnia* and *Temora* experiments.

1. Verify that the *velocity distribution* is Maxwellian. This confirms (in the absence of an independent measure of the excitation variance B) the *kinetic energy balance* of Equation 11.10.
2. Calculate the *velocity autocorrelation* $R(\tau)$, and verify that its form fits the kinematic requirement illustrated in Figure 11.1.

   Fit $R(\tau)$ to find ω and k. This is done by minimizing, by inspection, the square-error function:

$$J(\omega,k)=\sum_{\tau}\left(R_{observed}(\tau)-R_{theoretical}(\tau)\right)^2 \tag{11.22}$$

   With these parameters, directly integrate Equation 11.4 to create a simulated ensemble of velocity autocorrelations, and thus a numerical prediction of the autocorrelation *variance* (just as Equation 11.5 gives an analytical prediction for the autocorrelation *mean*).
3. With ω from step 2, confirm the *relation between swarm size and kinetic energy* predicted by Equation 11.12.
4. Compare the *mean and variance of the spatial acceleration field* with those predicted by Equations 11.16 and 11.23.
5. Examine *motion in the z (vertical, along-laser) direction,* which we have not to this point discussed. In this dimension the attractor is more-or-less isotropic and we might expect diffusive, not swarming, dynamics. The animals' vertical motion can be compared with theory under the assumption that the diffusion-driven parameters $\overline{u^2}$, B, and k will be the same in the z direction as they are in the x and y (cross-laser, swarming) directions. Here we follow an abbreviated version of the outline above.

   Look for a Maxwellian *velocity distribution,* as in step 1.

   Calculate the *velocity autocorrelation,* compare its ensemble *mean* with Equation 11.8, and compare its ensemble *variance* with numerical results, as in step 2.

   Calculate the *mean and variance of the acceleration field* as in step 4. We now expect the mean to be zero (by Equation 11.16, with $\omega=0$) and the variance to be as predicted by Equation 11.19.

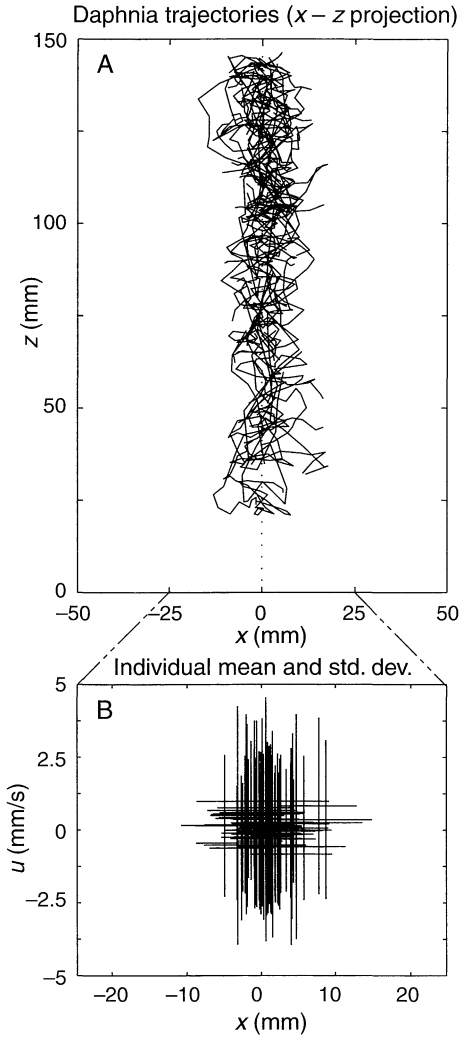

FIGURE 11.3 (A) Superimposition of all 58 *Daphnia* trajectories included in the analysis, shown in x–z projection. Plot boundaries indicate the edges of the tank, and the dotted line shows the position of the light shaft. (B) Position (horizontal axis) and velocity (vertical axis) statistics for each trajectory sample. The crosshairs, each representing a single animal trajectory, are centered on the mean horizontal position and velocity, and indicate standard deviations by their extent.

11.5 Results

Results for the *Daphnia* experiment are shown in Figure 11.5 and results for *Temora* in Figure 11.6. Note that the calculations for the horizontal dimensions in the *Temora* data are two dimensional, as both horizontal components of motion were captured and analyzed, and one dimensional for the *Daphnia* data. The parameters k, ω, and B, derived from the horizontal analysis, along with rms velocity and position (which represent u^2 and x^2), are summarized for both species in Table 11.1. Also given are rms positions (i.e., swarm sizes) predicted by Equation 11.12 and the error between these predictions and the values observed.

11.5.1 Velocity Distributions

Figure 11.5A, B and Figure 11.6A, B show observed velocity distributions for the horizontal (swarming) and vertical (diffusive) dimensions, along with theoretical curves based on Equations 11.11 and 11.15.

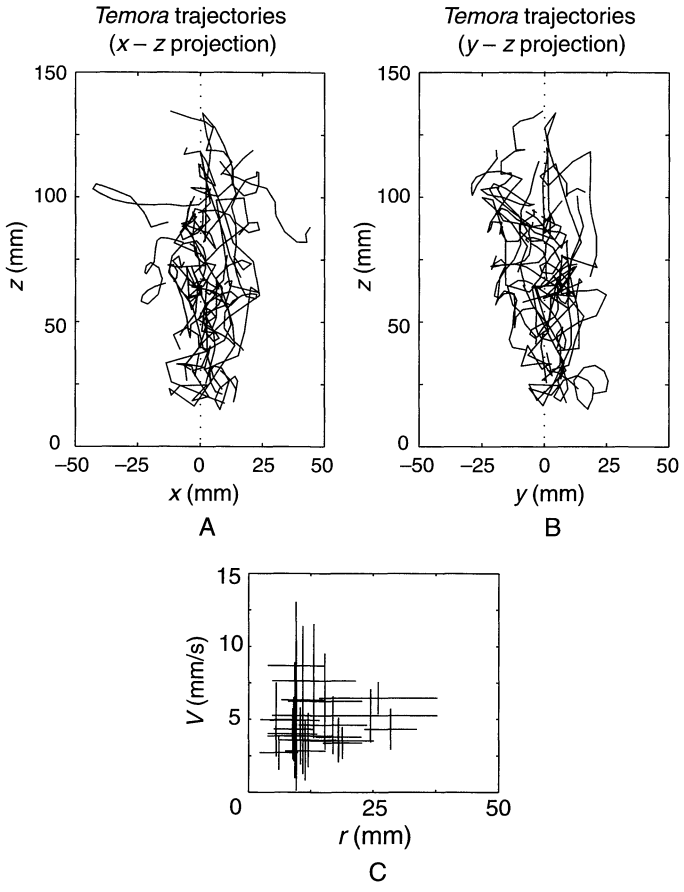

FIGURE 11.4 (Superimposition of the 20 *Temora* trajectories included in the analysis, shown in (A) x–z and (B) y–z projection. Plot boundaries indicate the edges of the tank, and the dotted line shows the position of the light shaft. (C) Position (horizontal axis) and velocity (vertical axis) statistics for each trajectory sample. The crosshairs, each representing a single animal trajectory, are centered on the mean horizontal position and velocity, and indicate standard deviations by their extent.

All velocity fields are close to stationary ($\bar{u}^2 << \overline{u^2}$). Velocity distributions for both species lie close to the predicted Maxwellian curves, with $r^2 = 0.65$ and 0.98 for the horizontal and vertical axes of the *Daphnia* motion and $r^2 = 0.91$ and 0.86 for the horizontal and vertical axes for *Temora*. The horizontal *Daphnia* distribution is more platykurtic than predicted, and the horizontal *Temora* distribution more sharply peaked, but these deviations could be either statistical artifacts or true dynamic effects related to these species' swimming styles, and are second-order effects in either case. The first-order match with theory supports our assumption of a Stokes form for drag and a stochastic, spatially symmetrical excitation.

Note also that, with the exception of a possible upward drift along the laser axis in the *Temora* data (Figure 11.6B), the velocity fields are very close to symmetrical, and that velocity variances are similar, for each animal, in the horizontal and vertical dimensions. In fact, velocity variances are indistinguishable for the two horizontal dimensions in the *Temora* data ($\overline{u^2} = 16.7$ mm^2/s^2, $\overline{v^2} = 16.6$ mm^2/s^2). These patterns support the spatial symmetries we have assumed and our supposition of dynamic consistency between the along-laser and cross-laser diffusion processes. Note that an upward drift in the *Temora* experiment would be consistent with a weak phototactic response to the attenuation of the light shaft through the water column.

11.5.2 Velocity Autocorrelations and Fit Parameters

Figure 11.5C, D show observed and theoretical velocity autocorrelations for the two dimensions of *Daphnia* motion. The horizontal theoretical mean is a fit to the data shown, while the vertical theoretical

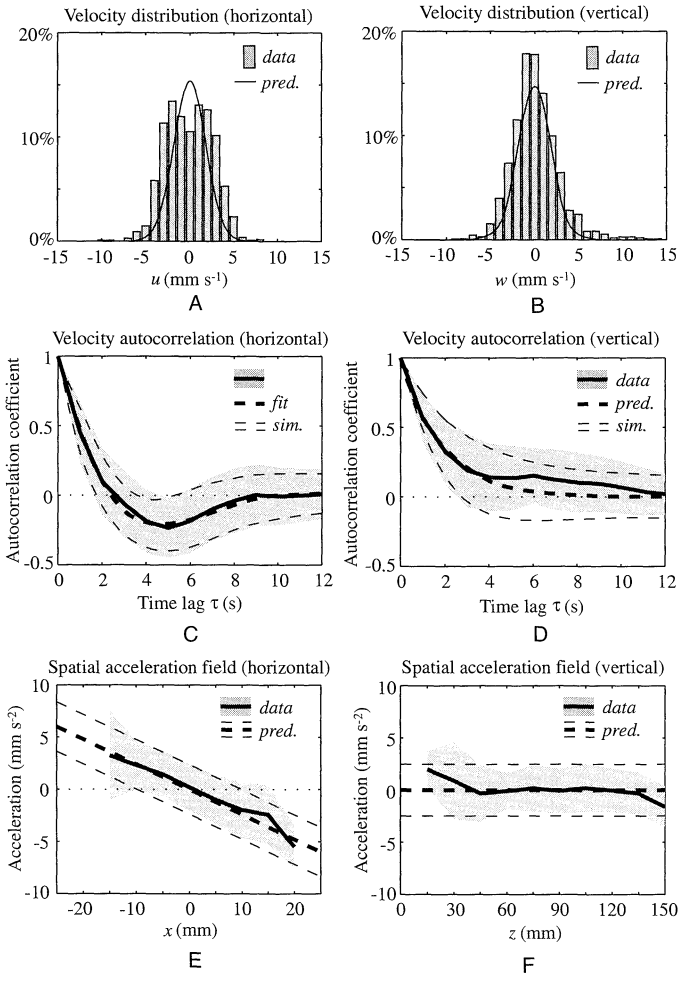

FIGURE 11.5 Results for *Daphnia*. Velocity distributions (A, B), velocity autocorrelations (C, D), and acceleration fields (E, F) for the horizontal (A, C, E) and vertical (B, D, F) axes of motion. In all panels, thick lines indicate means and shaded areas and thin dotted lines indicate standard deviations. Full explanations of plotted quantities are given in the text.

mean is not a fit but a prediction based on Equation 11.8 with k from the horizontal analysis. Theoretical standard deviations are calculated from numerical simulation. Figure 11.6C, D show autocorrelations for *Temora* in the same format, except that here the observed horizontal velocity autocorrelation (Figure 11.6C) is the average of the x and y autocorrelations, a quantity that is invariant under rotation of the horizontal axes.

Horizontal autocorrelations for both species are fit very closely by theoretical curves (*Daphnia*, r^2 = 0.995; *Temora*, r^2 = 0.90). This match is a strong validation of the kinematic theory underlying our analysis. Variance of individuals around the ensemble mean for each species is close to the level that simulation predicts (*Daphnia*, r^2 = 0.95; *Temora*, r^2 = 0.71). Note that in contrast to the underdamped, highly orbital trajectories of members of the midge swarm analyzed by Okubo and Anderson (1984), both the *Daphnia* and *Temora* swarms appear to be near critical damping, with individuals' velocities decorrelating almost entirely in less than one period of the harmonic attractive force.

Values of k derived from the horizontal swarming motion suggest decaying autocorrelation curves for the vertical motion that correspond well with observations (Figure 11.5D and Figure 11.6D), confirming our supposition that motion along the laser axis is primarily random and diffusive, and that the same damping force acts on horizontal and vertical swimming. The *Daphnia* vertical autocorrelation, however, has a longer tail than predicted, suggesting that the animals tend to drift, actively or passively, along the

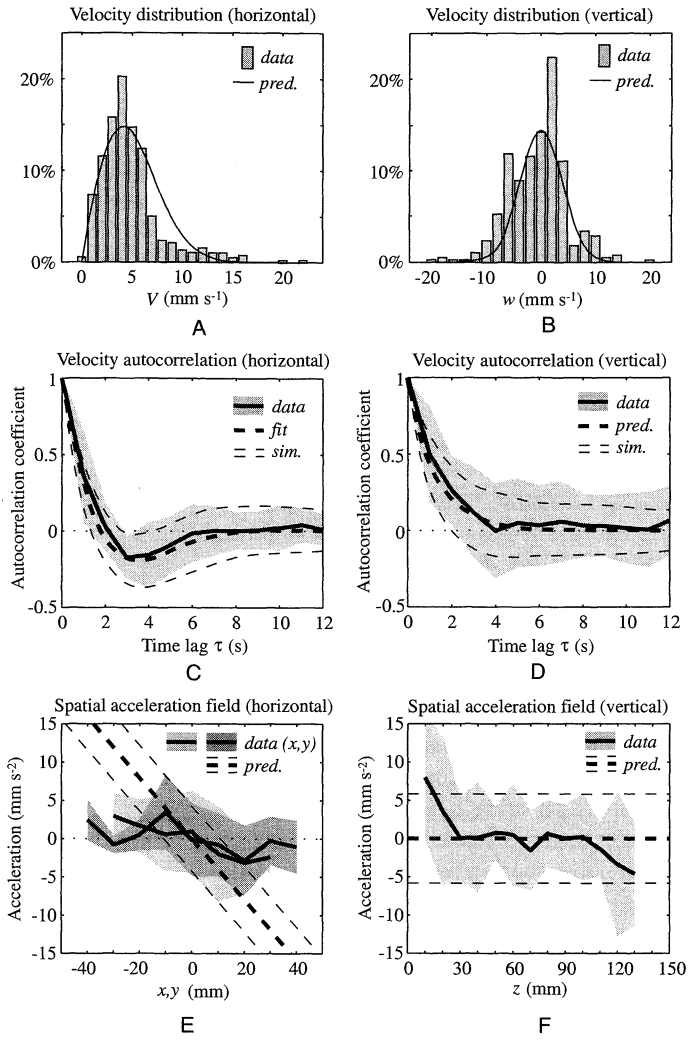

FIGURE 11.6 Results for *Temora*. Velocity distributions (A, B), velocity autocorrelations (C, D), and acceleration fields (E, F) for the horizontal (A, C, E) and vertical (B, D, F) axes of motion. In all panels, thick lines indicate means and shaded areas and thin dotted lines indicate standard deviations. Full explanations of plotted quantities are given in the text.

laser axis, in combination with their diffusive behavior. The *Temora* vertical autocorrelation may or may not indicate the same tendency.

Fitting the horizontal autocorrelations for k and ω lets us test the consistency of the theoretical relationship (Equation 11.12) between swarm size, swimming speed, and the strength of the concentrative force. Table 11.1 gives observed and predicted values of the swarm size for both species. They agree — i.e., the relationship between parameters is consistent with theory — to 4% for *Daphnia* and 45% for *Temora*.

11.5.3 Acceleration Fields

Figure 11.5E, F and Figure 11.6E, F show the observed acceleration fields with theoretical means and standard deviations from Equations 11.16 and 11.19. The x and y acceleration fields for *Temora* (Figure 11.6E) are superimposed.

The horizontal *Daphnia* acceleration field (Figure 11.5E) agrees well with theory in both its mean slope (which is not significantly different from the predicted value of zero) and its mean standard

TABLE 11.1

Dynamic and Kinematic Parameters along the Axes of Swarming Motion for the *Daphnia* and *Temora* Experiments

		Source	*Daphnia*	*Temora*
Damping coefficient	k	Fit to velocity autocorrelation	0.54 s^{-1}	0.80 s^{-1}
Concentration coefficient	w	Fit to velocity autocorrelation	0.49 s^{-1}	0.63 s^{-1}
Power of excitation	B	Equations 11.10, 11.13	3.6 $mm^2\ s^{-3}$	13.3 $mm^2\ s^{-3}$
Kinetic energy	$\sqrt{\overline{u^2}}$	Observed	2.6 mm s^{-1}	
(rms velocity)	$\sqrt{\overline{u^2} + \overline{v^2}}$			5.8 mm s^{-1}
Swarm radius	$\sqrt{\overline{x^2}}$	Observed	5.5 mm	
(rms position)	$\sqrt{\overline{x^2} + \overline{y^2}}$			16.6 mm
Predicted swarm radius	$\sqrt{\overline{x^2}}_{pred}$	Equation 11.12	5.3 mm	
	$\sqrt{\overline{x^2} + \overline{y^2}}_{pred}$	Equation 11.14		9.1 mm
Error in swarm size (observed–predicted)			4%	45%

deviation (error = 11%). The vertical *Daphnia* acceleration field (Figure 11.5F) shows similar agreement (error in mean standard deviation = 8.9%), although superimposed on the diffusive field are an upward mean acceleration near the bottom of the tank and a downward mean near the top. These perturbations suggest that the animals feel the top and bottom boundaries of the domain, perhaps hydrodynamically, and turn away from them. The vertical *Temora* acceleration field suggests the same behavior.

The variances of the *Temora* acceleration fields are similar to those predicted by our random-flight model (error in mean standard deviation 2.2% for the x direction, 30% for y, 11% for z), but the horizontal mean field is much smaller than predicted. In the absence of other results this might be taken to mean the absence of a concentrative acceleration and thus primarily diffusive behavior, but the horizontal velocity autocorrelation (Figure 11.6C) suggests a swarming balance very strongly. Instead, we attribute the poor definition of the mean horizontal *Temora* acceleration field to noise in the data, i.e., a combination of sampling error and real, high-speed behaviors not accounted for by our model. There are several reasons to suspect this type of error. The *Temora,* unlike the *Daphnia,* make their turns quickly, generally in less than the sampling time step of 1 s. Their trajectories wobble and jitter at high (~10 Hz) frequencies, in ways that may be related to the trail-following that Weissburg et al. (1998) observed in the same series of *Temora* experiments. Furthermore, in general, successive derivatives of a data set (calculation of the acceleration requires two) amplifies noise at the high-frequency end of a power spectrum. One would expect a moderate level of noise in the acceleration field to wash out the small mean field but have only a secondary effect on the field's variance, as is observed.

11.6 Discussion

11.6.1 Model Consistency

Our goal here has been to provide an internally consistent model description of a steady-state zooplankton swarm, by a method that could be applied generally to the problem of assessing physical and biological controls on zooplankton aggregation. The analysis above verifies the suitability of the model presented here to the artificially stimulated swarms we have described. It also suggests the level of quantitative agreement we can expect for real organisms, which do not move like idealized particles and inevitably are engaged in other behaviors at the same time they are swarming: errors up to a factor of two, with closer correspondences in most measures. The median unexplained variance ($1 - r^2$) for all theoretical fits for which it was calculable was 11%.

For many purposes, high-precision agreement with data may not actually make a descriptive model any more *useful* than one with moderate-precision agreement. This is especially true for a problem like zooplankton aggregation, in which the parameters of ultimate interest — number densities and encounter rates — vary over several orders of magnitude. Nevertheless, higher-frequency sampling or more involved frequency-domain filtering might reduce errors in laboratory results, by suppressing sampling error and isolating swarming motion from other behaviors more precisely. It appears, however, that in the present study — perhaps for models that entail strongly stochastic behavior in general — larger sample sizes would not. Variations in individual behavior around the ensemble mean are substantial — this is most visible in the velocity autocorrelations (Figure 11.5C and Figure 11.6C) — but this variation is not significantly greater than what the model dynamics predict, suggesting that in a larger ensemble the mean would be no more precisely defined.

Figure 11.7 shows individual velocity autocorrelations for 36 *Daphnia* trajectories, selected at random out of the full set of 58 for illustrative purposes, and for comparison 36 autocorrelations numerically that were simulated using the momentum Equation 11.4 and fit values of ω and k. Only a few of the observed individual trajectories actually match the ensemble average (Figure 11.5C) in form; those that do suggest orbital periods (i.e., values of ω) and decorrelation times (i.e., values of k) that vary by an order of magnitude. Just as many records appear to decorrelate within a few seconds, suggesting no easily describable kinematic pattern thereafter. What is significant here is that all these forms for the autocorrelation appear among the simulated trajectories as well. Because of the inherent stochastic element in this motion, a single dynamic balance with a single set of parameters can produce what appears to be a wide variety of individual behaviors. Note also the common element in these variegated trajectories: all satisfy the kinematic requirement for swarming, illustrated in Figure 11.1, that their autocorrelations integrate to a value near zero.

11.6.2 Model Interpretation

A number of physical or biological interpretations are possible for each of the terms in our model Equation 11.4, and thus we have so far left the meaning of these terms very general. Clearly, the strict Newtonian interpretation — external forces incident upon a passive particle — is insufficient in our experiment, although this interpretation might sometimes be appropriate for animals in a more energetic and complex environment than our placid laboratory tank: plankton who live up to their Greek name and simply drift. In general, however, each of the force terms in Equation 11.4 can be given either a physical or a behavioral interpretation:

11.6.2.1 Damping — The damping $-ku$ may represent viscous drag, here assumed to obey Stokes' law to keep the model linear, although Okubo and Anderson (1984) note that this may not be the right form of drag for large and fast-moving zooplankton. Alternatively, it could represent a decorrelative behavior, akin to the tendency of many zooplankton to turn more often in a food patch (Williamson, 1981; Buskey, 1984; Price, 1989; McGehee and Jaffe, 1996).

An estimate of hydrodynamic drag on the animals in our experiment suggests the behavioral interpretation. Assume that the damping $-ku$ is a linearization of a more realistic and more widely applicable quadratic drag law, so that

$$-ku \sim \frac{1}{2}\frac{C_d \rho_w A u^2}{V \rho_z} \tag{11.23}$$

(Haury and Weihs, 1976) and

$$k \sim \frac{1}{2} C_d \frac{\rho_w}{\rho_z}\frac{A}{V} u \tag{11.24}$$

where u is the velocity, V the volume, A the frontal cross section, ρ_z the density, and C_d the drag coefficient of a zooplankter moving through water of density ρ_w. We can assume that the ratio of water to animal

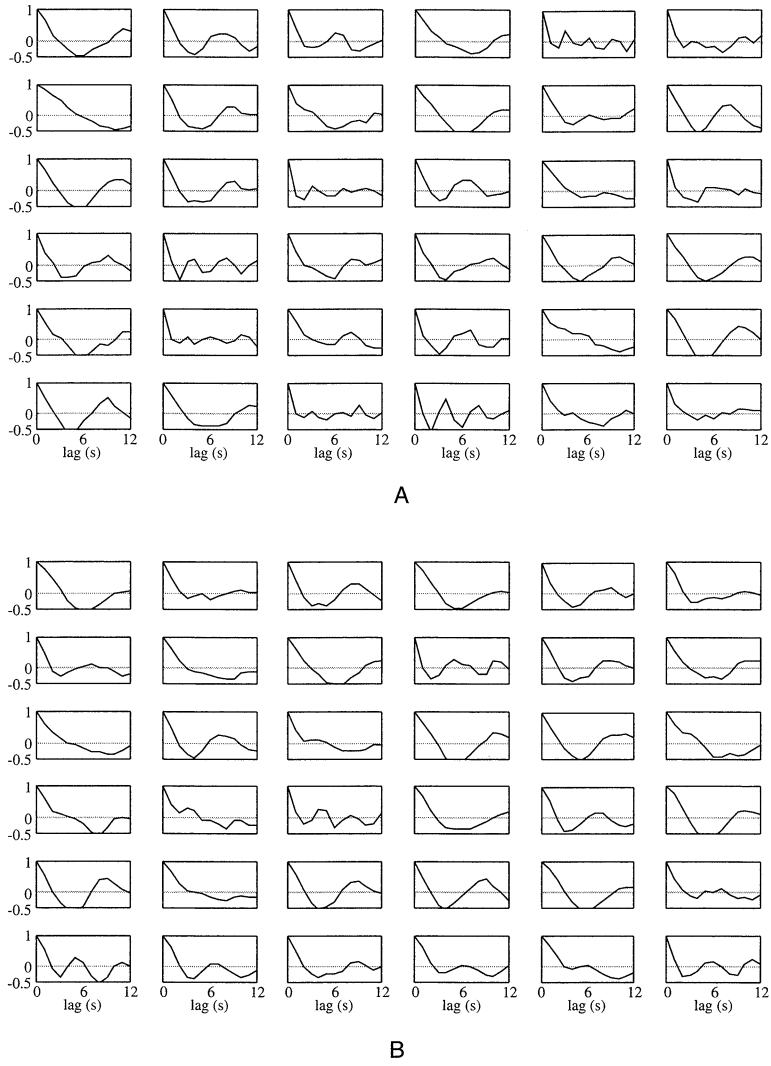

FIGURE 11.7 Individual horizontal velocity autocorrelations, selected from the ensemble at random, for (A) *Daphnia* and (B) numerically simulated *Daphnia*.

density is O(1), and estimate the ratio of volume to frontal area as body length l. Drag coefficients are a function of Reynolds number:

$$\mathrm{Re} \equiv \frac{ul}{\nu} \tag{11.25}$$

where ν is the dynamic viscosity of seawater, $\sim 10^{-6}$ m^2 s^{-1}, and we have assumed that body length and diameter are similar. For the animals in our experiment (*Daphnia:* $u \sim 3$ mm s^{-1}, $l \sim 3$ mm; *Temora:* $u \sim 6$ mm s^{-1}, $l \sim 1$ mm; Yen et al., 1998), Re is between 1 and 10, values for which observations of zooplankton suggest $C_d \sim 10$ or higher (Haury and Weihs, 1976). Thus, for both *Daphnia* and *Temora,* a low estimate for the effective Stokes coefficient is $k \sim 10$ s^{-1}.

This is fully an order of magnitude larger than the k values associated with swarming in our experiment (Table 11.1). In other words, hydrodynamic drag appears to operate here at a timescale $1/k$ much shorter than the timescale of swarming motion, indeed much shorter than our sampling interval of 1 s. While drag may well be important in the dynamics of avoidance reactions between

the swarmers, trail-following, rapid changes of direction, and the like, it does not appear to have explicit effects in the regime of motion we have been considering. Thus the damping of forward motion that limits the energy and spatial extent of the *Daphnia* and *Temora* swarms appears to be not passive and fluid mechanical, but rather active and behavioral, a tendency consistent with the classical "area-restricted search" model of Tinbergen et al. (1967).

11.6.2.2 Excitation — The excitation $A(t)$ clearly is behavioral in our experiment, since the background flow field is negligible, but one could also model turbulent dispersion through this term. Indeed, the kinematic approach of our model does not differentiate between dispersion by behavior and dispersion by the environment, and thus it lets one express observations of excitational behavior in a form directly comparable with standard turbulence formulations. In the absence of an aggregative tendency (that is, with $\omega = 0$), Equations 11.2 and 11.8 predict that a swarm will disperse with a diffusivity

$$D = \overline{u^2} \int R(\tau) d\tau \sim \frac{\overline{u^2}}{k} \tag{11.26}$$

For our *Daphnia* and *Temora* swarms, for example, this (behavioral) diffusivity is 10^{-6} to 10^{-5} m^2 s^{-1}, similar to background diapycnal diffusivities in the open ocean (Gregg et al., 1999). This comparison is simply illustrative and is not meant to measure the ability of these animals to aggregate against turbulence, as they do not appear to be swimming at capacity here: *Temora,* for example, have been observed to lunge at speeds more than ten times the rms velocity of the swarmers we have described (Doall et al., 1998). Yamazaki and Squires (1996) find that most zooplankton swim at speeds greater than or comparable to the velocity fluctuations associated with upper-ocean turbulence.

11.6.2.3 Concentrative Force — The concentrative force $-\omega^2 x$ represents phototaxis in our experiments and, indeed, is likely to represent a behavioral response like phototaxis or chemotaxis in most physical environments. There are important exceptions, however: fronts from river plumes (e.g., Mackas and Louttit, 1988), Langmuir circulations (Stavn, 1971), and internal waves (Shanks, 1985) have all been found to cause passive aggregation as well. These physical mechanisms, which generally consist of advection by a convergent flow field, may not be represented well by the harmonic restoring force that our model employs.

11.6.2.4 Physical–Behavioral Balances — In summary, these possibilities suggest three principal balances of physical and biological processes to which the "aggregating random-walk" model could be applied:

1. Aggregative behavior, which maintains high animal concentrations against turbulent dispersion (as, for example, Tiselius et al. [1994] observed in a thin layer at a sharp pycnocline)
2. Dispersive behavior, which limits animal concentrations in a region of convergent flow (perhaps similar to the maintenance of nearest-neighbor distance by avoidance reaction observed by Leising and Yen, 1997)
3. A pure balance of aggregative and dispersive behaviors in a quiescent environment

Note that while so far we have discussed the excitational and concentrative forces as separate processes, we might also interpret them as mathematically paired components of a single swarming behavior: a behavior better described as a *spatial gradient in excitation.* (Spatial variations in eddy diffusivity are thought to cause anisotropic tracer distributions in the ocean [Armi and Haidvogel, 1982], and Mullen [1989] models fish dispersal and abundance using a variable diffusivity proportional to saturation of local carrying capacity.) This interpretation allows the possibility of a conceptually simple link between the gradient in stimulus (say, light intensity or chemical concentration) and a gradient in the behavioral response.

11.7 Conclusion

The members of phototactic swarms of *Daphnia* and *Temora* in the laboratory are found to follow, to first order, the dynamics of randomly diffusing particles subject to a linear restoring force. This behavioral model is found to fit the data to within ~10 to 20% overall. Larger errors, attributed to sampling method and unmodeled behaviors, occur in some measures of the *Temora* acceleration field and spatial distribution, but much closer matches (errors of 0.5 to 10%) are found in several fundamental kinematic measures: most notably, the form of the velocity autocorrelation along the axes of swarming motion.

In these experiments the concentrative force and diffusive excitation are individual behavioral responses to a stable environmental stimulus. In other circumstances, the same model dynamics could represent a variety of balances of physical accelerations like turbulence, drag, and flow convergence; individual responses to environmental cues; and interaction between swarm members.

The environmental and intraspecies cues that initiate individual swarming behaviors are varied and not well understood. A natural continuation of the laboratory experiments described above would be to investigate the effects of variations in the swarm stimulus (weaker and stronger light gradients, chemical and hydrodynamic cues) and the swarm demographics (species, life stage, physiological state, presence of predators, density, and so on.) One could also analyze *in situ* observations of zooplankton swarms in similar terms, and through this model draw inferences, in both directions, between individual behavior on the small scale and the dynamics of patches on the large scale.

Without further elaboration the model we have been considering makes no predictions about the outcome of such a series of observations. The benchmarks this model proposes, however — the form of the velocity autocorrelation and acceleration field; the parameters k, ω, and B, which index the strength of the forces which must balance to produce a stable swarm — are likely to clarify the role of behavior in maintaining zooplankton aggregations, as well as help identify the sensory pathways through which swarming zooplankton organize their environment. Thus we propose the zooplankton-swarming model discussed above not as a hypothesis concerning these problems, but as a mathematical language in which to pose the specific behavioral questions that experiment and ethology can answer.

Acknowledgments

This work was supported by National Science Foundation OCE-9314934 and OCE-9723960. N. Banas was partially supported by the Ward and Dorothy Melville Summer Research Fellowship at the Marine Sciences Research Center at the State University of New York at Stony Brook. Many thanks to J.R. Strickler, who generously provided the *Daphnia* data.

References

Alldredge, A., Robison, B., Fleminger, A., Torres, J., King, J., and Hamner, W.M. 1984. Direct sampling and *in situ* observation of a persistent copepod aggregation in the mesopelagic zone of the Santa Barbara Basin. *Mar. Biol.,* 80: 75–81.

Ambler, J.W., Ferrari, F.D., and Fornshell, J.A. 1991. Population structure and swarm formation of the cyclopoid copepod *Dioithona oculata* near mangrove cays. *J. Plankton Res.,* 13: 1257–1272.

Armi, L. and Haidvogel, D.B. 1982. Effects of variable and anisotropic diffusivities in a steady-state diffusion model. *J. Phys. Oceanogr.,* 12: 785–794.

Bollens, S.M., Frost, B.W., and Cordell, J.R. 1994. Chemical, mechanical and visual cues in the vertical migration behavior of the marine planktonic copepod *Acartia hudsonica. J. Plankton Res.,* 16: 555–564.

Brandl, Z. and Fernando, C.H. 1971. Microaggregation of the cladoceran *Ceridaphnia affinis* Lilljeborg with a possible reason for microaggregation of zooplankton. *Can. J. Zool.,* 49: 775.

Bundy, M.H., Gross, T.F., Coughlin, D.J., and Strickler, J.R. 1993. Quantifying copepod searching efficiency using swimming pattern and perceptive ability. *Bull. Mar. Sci.,* 53: 15–28.

Buskey, E.J. 1984. Swimming pattern as an indicator of the roles of copepod sensory systems in the recognition of food. *Mar. Biol.,* 79: 165–175.

Buskey, E.J., Peterson, J.O., and Ambler, J.W. 1995. The role of photoreception in the swarming behavior of the copepod *Dioithona oculata. Mar. Freshw. Behav. Physiol.,* 26: 273–285.

Clements, A.N. 1963. *The Physiology of Mosquitoes.* Pergamon Press, Oxford.

Davis, C.S., Flierl, G.R., Wiebe, P.H., and Franks, P.J.S. 1991. Micropatchiness, turbulence, and recruitment in plankton. *J. Mar. Res.,* 49: 109–151.

Davis, C.S., Gallager, S.M., and Solow, A.R. 1992. Microaggregations of oceanic plankton observed by towed video microscopy. *Science,* 257: 230–232.

Doall, M.H., Colin, S.P., Strickler, J.R., and Yen, J. 1998. Locating a mate in 3D: the case of *Temora longicornis. Philos. Trans. R. Soc. London B,* 353: 681–689.

Eloffson, R. 1966. The nauplius eye and frontal organs of the non-malacostraca (Crustacea). *Sarsia,* 25: 1–128.

Fields, D.M. and Yen, J. 1997. The escape behavior of marine copepods in response to a quantifiable fluid mechanical disturbance. *J. Plankton Res.,* 19: 1289–1304.

Gallager, S.M., Davis, C.S., Epstein, A.W., Solow, A., and Beardsley, R.C. 1996. High-resolution observations of plankton spatial distributions correlated with hydrography in the Great South Channel, Georges Bank. *Deep-Sea Res.,* 43: 1627–1663.

Gendron, D. 1992. Population structure of daytime surface swarms of *Nyctiphanes simplex* (Crustacea: Euphausiacea) in the Gulf of California, Mexico. *Mar. Ecol. Prog. Ser.,* 87: 1–6.

Goldsmith, A., Chiang, H.C., and Okubo, A. 1980. Turning motion of individual midges, *Anarete pritchardi,* in swarms. *Ann. Entomol. Soc. Am.,* 73: 526–528.

Gregg, M.C., Winkel, D.W., MacKinnon, J.A., and Lien, R.-C. 1999. Mixing over shelves and slopes. *'Aha Huliko'a Proceedings, Hawaiian Winter Workshop,* P. Muller and D. Henderson, Eds., University of Hawaii, 35–42.

Grünbaum, D. 1994. Translating stochastic density-dependent individual behavior with sensory constraints to an Eulerian model of animal swarming. *J. Math. Biol.,* 33: 139–161.

Hamner, W.M. and Carlton, J.H., 1979. Copepod swarms: attributes and role in coral reef ecosystems. *Limnol. Oceanogr.,* 24: 1–14.

Hamner, W.M., Hamner, P.P., Strand, S.W., and Gilmer, R.W. 1983. Behavior of Antarctic krill *Euphausia superba:* chemoreception, feeding, schooling, and molting. *Science,* 220: 433–435.

Hanson, A.K. and Donaghay, P.L. 1998. Micro- to fine-scale chemical gradients and layers in stratified coastal waters. *Oceanography,* 11: 10–17.

Haury, L. and Weihs, D. 1976. Energetically efficient swimming behavior of negatively buoyant zooplankton. *Limnol. Oceanogr.,* 21: 797–803.

Hebert, P.D.N., Good, A.G., and Mort, M.A. 1980. Induced swarming in the predatory copepod *Heterocope septentrionalis. Limnol. Oceanogr.,* 25: 747–750.

Hussussian, G., Yen, J., and Strickler, J.R. 1993. Digitized data from 1993 experiments on swarming in *Daphnia magna.* Special report 47, Center for Great Lake Studies, Milwaukee, WI, 48 pp.

Katona, S.K. 1973. Evidence for sex pheromones in planktonic copepods. *Limnol. Oceanogr.,* 18: 574–583.

Lasker, R. 1975. Field criteria for survival of anchovy larvae: the relation between inshore chlorophyll maximum layers and successful first feeding. *Fish. Bull.,* 73: 453–462.

Leising, A.W. and Yen, J. 1997. Spacing mechanisms within light-induced copepod swarms. *Mar. Ecol. Prog. Ser.,* 155: 127–135.

Mackas, D.L. and Louttit, G.C. 1988. Aggregation of the copepod *Neocalanus plumchrus* at the margin of the Fraser River plume in the Strait of Georgia. *Bull. Mar. Sci.,* 43: 810–824.

McGehee, D. and Jaffe, J. 1996. Three-dimensional swimming behavior of individual zooplankters: observations using the acoustical imaging system FishTV. ICES *J. Mar. Sci.,* 53: 363–369.

Mullen, A.J. 1989. Aggregation of fish through variable diffusivity. *Fish. Bull.,* 8: 353–362.

Okubo, A. 1980. *Diffusion and Ecological Problems: Mathematical Models.* Springer-Verlag, Berlin, 254 pp.

Okubo, A. 1986. Dynamical aspects of animal grouping: swarms, schools, flocks and herds. *Adv. Biophys.,* 22: 1–94.

Okubo, A. and Anderson, J.J. 1984. Mathematical models for zooplankton swarms: their formation and maintenance. *Eos,* 65: 731–732.

Poulet, S.A. and Ouellet, G. 1982. The role of amino acids in the chemosensory swarming and feeding of marine copepods. *J. Plankton Res.,* 4: 341–361.

Price, H.J. 1989. Swimming behavior of krill in response to algal patches: a mesocosm study. *Limnol. Oceanogr.,* 34: 649–659.

Russell, F.S. 1934. The vertical distribution of marine macroplankton. XII. Some observations on the vertical distribution of *Calanus finmarchicus* in relation to light intensity. *J. Mar. Biol. Assoc. U.K.,* 19: 569–584.

Schultze, P.C., Strickler, J.R., Bergström, B.I., Donaghay, P.C., Gallager, S., Haney, J.F., Hargreaves, B.R., Kils, U., Paffenhöfer, G.-A., Richman, S., Vanderplo, E.G., Welsch, W., Wethey, D., and Yen, J. 1992. Video systems for *in situ* studies of zooplankton. *Arch. Hydrobiol. Beih. Erg. Limnol.,* 36: 1–21.

Shanks, A.L. 1985. Behavioral basis of internal-wave-induced shoreward transport of megalopae of the crab *Pachygraspus crassipes*. *Mar. Ecol. Prog. Ser.,* 24: 289–95.

Smith, S.L., Pieper, R.E., Moore, M.V., Rudstam, L.G., Greene, C.H., Zamon, J.E., Flagg, C.N., and Williamson, C.E. 1992. Acoustic techniques for the *in situ* observation of zooplankton. *Arch. Hydrobiol. Beih.,* 36: 23–43.

Stavn, R.H. 1971. The horizontal-vertical distribution hypothesis: Langmuir circulations and *Daphnia* distributions. *Limnol. Oceanogr.,* 16: 453–466.

Stearns, S.C. 1975. Light responses of *Daphnia pulex*. *Limnol. Oceanogr.,* 20: 564–570.

Strickler, J.R. 1998. Observing free-swimming copepods mating. *Philos. Trans. R. Soc. London B,* 353: 671–680.

Strickler, J.R. and Hwang, J.-S. 1998. Matched spatial filters in long working distance microscopy of phase objects. In *Focus on Multidimensional Microscopy,* P.C. Cheng, P.P. Hwang, J.L. Wu, G. Wang, and H. Kim, Eds., World Scientific, River Edge, NJ.

Tinbergen, N., Impekoven, M., and Franck, D. 1967. An experiment on spacing-out as a defense against predation. *Behaviour,* 28: 207–321.

Tiselius, P. 1992. Behavior of *Acartia tonsa* in patchy food environments. *Limnol. Oceanogr.,* 37: 1640–1651.

Tiselius, P., Nielsen, G., and Nielsen, T.G. 1994. Microscale patchiness of plankton within a sharp pycnocline. *J. Plankton Res.,* 16: 543–554.

Ueda, H., Kuwahara, A., Tanaka, M., and Azeta, M. 1983. Underwater observations on copepod swarms in temperate and subtropical waters. *Mar. Ecol. Prog. Ser.,* 11: 165–171.

Uhlenbeck, G.E. and Ornstein, L.S. 1930. On the theory of the Brownian motion. *Phys. Rev.,* 36: 823–841.

Weissburg, M.J., Doall, M.H., and Yen, J. 1998. Following the invisible trail: mechanisms of chemosensory mate tracking by the copepod *Temora longicornus*. *Philos. Trans. R. Soc. London B,* 353: 701–712.

Williamson, C. 1981. Foraging behavior of a freshwater copepod: frequency changes in looping behavior at high and low prey densities. *Oecologia,* 50: 332–336.

Wishner, K., Durbin, E., Durbin, A., Macaulay, M., Winn, H., and Kenney, R. 1988. Copepod patches and right whales in the Great South Channel off New England. *Bull. Mar. Sci.,* 43: 825–844.

Yamazaki, H. 1993. Lagrangian study of planktonic organisms: perspectives. *Bull. Mar. Sci.,* 53: 265–278.

Yamazaki, H. and Okubo, A. 1995. A simulation of grouping: an aggregating random walk. *Ecol. Modelling,* 79: 159–165.

Yamazaki, H. and Squires, K.D. 1996. Comparison of oceanic turbulence and copepod swimming. *Mar. Ecol. Prog. Ser.,* 144: 299–301.

Yen, J. and Bundock, E.A. 1997. Aggregative behavior in zooplankton: phototactic swarming in four developmental stages of *Coullana canadensis* (Copepoda, Harpacticoida). In *Animal Groups in Three Dimensions,* J. Parrish and W. Hamner, Eds., Cambridge University Press, New York, 143–162.

Yen, J., Weissburg, M.J., and Doall, M.H. 1998. The fluid physics of signal perception by mate-tracking copepods. *Philos. Trans. R. Soc. London B,* 353: 787–804.

Yoder, J.A., Ackleson, S.G., Barber, R.T., Flament, P., and Balch, W.M. 1994. A line in the sea. *Nature,* 371: 689–692.